INTERNATIONAL JOURNAL FOR NUMERICAL METHODS IN FLUIDS, VOL. 23, 1021–1041 (1996)

NUMERICAL STUDY OF STEADY LAMINAR FLOW THROUGH TUBES WITH MULTIPLE CONSTRICTIONS USING CURVILINEAR CO-ORDINATES

V. DAMODARAN, G.W. RANKIN AND C. ZHANG

Department of Mechanical Engineering and Fluid Dynamics Research Institute, University of Windsor, Windsor, Ontario, Canada

SUMMARY

The flow field through tubes with multiple axisymmetric constrictions in tubes was studied numerically. Two practical problem cases were considered and the numerical scheme was developed for both. In the first case there are one, two, three and four constrictions in the tube. The effects of the number of constrictions on wall shear stress, pressure drop, streamline, vorticity and velocity distributions as the flow passes through the tube were studied and the development of the periodicity characteristics was investigated. In the second case there were multiple constrictions in the tube equidistant from each other. For this case the governing equations were reformulated for a module at a sufficient distance downstream from the inlet where the entrance region effects could be ignored and flow field is assumed to repeat itself. The flow field solutions were obtained in this region. The governing equations were formulated in curvilinear co-ordinates and a finite volume discretization procedure was used to solve the problem. The computations were carried out over a range of Reynolds numbers between 50 to 250 for constrictions with 75 percent area reduction. The method is validated by comparing some of the solutions with experimental results.

KEY WORDS: curvilinear co-ordinate system; constriction; stenosis; module; finite volume

INTRODUCTION

The effect of axisymmetric constrictions in tubes has many important applications especially in biofluids. The constriction of an artery commonly known as a stenosis is one of the most frequently occurring abnormalities in man. The results of a steady flow analysis for this situation is an important first step in studying the effects of arterial stenosis on the human body. Studies of the stenotic flow fields have been done by numerous investigators. The relevant work is mentioned here. Young and Tsai[1] conducted a series of steady flow experiments for various hydrodynamic factors such as pressure drop, separation and turbulence. Talukder *et al.*[2] conducted an experimental study of the effects of multiple stenoses on the pressure drop. Ahmed and Giddens[3] investigated the velocity field in the neighbourhood of axisymmetric constrictions. Experimental studies of stenotic blood flow have been augmented by theoretical models (e.g. Lee and Fung,[4] Deshpande *et al.*,[5] van Dreumel and Kuiken[6]). Lee[7] gave a numerical analysis of fluid flow through tubes with double constrictions. Angiograms taken from patients having coronary symptoms have shown the presence of several stenoses on the same artery. Configurations of tubes with multiple constrictions are also used in heat exchangers to enhance heat transfer. An example for such a system is a reflux condenser. Sparrow

CCC 0271–2091/96/101021–21

Received 5 June 1995
Revised 2 December 1995

and Prata[8] obtained a numerical solution for the heat transfer problem in the fully developed regime in a duct of periodically varying cross-section. They solved the problem for a module in the fully developed regime in polar co-ordinates by blocking the flow passage in such a manner that it approximates the geometry of a converging diverging duct and used the periodicity boundary conditions to solve the problem. Other related papers involving a similar approach include Prata and Sparrow[9] and Patankar *et al.*[10]

A review of the literature indicates that the average Reynolds number for the human carotid artery and the monkey aorta is usually less than 400 whereas for the human and dog aortas the averaged Reynolds number is less than 2000 (Ahmed and Giddens[3]). Talukder *et al.*[2] varied the Reynolds number between 30 and 280 in their experimental *in vitro* and *in vivo* studies. They selected this range to study the flow conditions encountered clinically. Their *in vivo* studies were conducted using the iliac and femoral arteries of an anaesthetized dog. These studies indicate that laminar flow studies are relevant for a number of the arteries in the human body. Accordingly, the numerical investigation presented here is restricted to steady laminar flow through a rigid tube which has one or more localized axisymmetric constrictions. For those cases where higher Reynolds number flows occur the question arises whether the flow is entirely turbulent and whether standard turbulence models can be used. The present work is conducted as a first step towards analysis of those cases.

The problem was solved by transforming the Navier–Stokes equation from polar co-ordinates into curvilinear co-ordinates and using a finite volume numerical method. Most of the earlier numerical work on these type of problems has been done using cylindrical polar co-ordinates or using a problem specific co-ordinate transformation. To our knowledge no numerical investigation has been attempted to study the flow characteristics for a single module in the fully developed region of a tube with multiple constrictions using curvilinear co-ordinates along with periodic boundary conditions. The use of a curvilinear co-ordinate system has many advantages. Application of cylindrical polar co-ordinates to curved surfaces usually involves interpolation between the grid points that are not coincident with the boundaries which may adversely affect the accuracy of the solution. The shape and the number of constrictions can also be varied without any changes in the numerical method with a curvilinear coordinate transformation.

The main objective of this paper is to provide a detailed analysis on the dynamics of the flow over a range of Reynolds numbers with constrictions of 75 per cent area reduction, and to observe the development of the periodicity characteristics of the flow. Constrictions of 75 per cent reduction in the flow area are selected as it is the commonly accepted critical value of stenosis.[2] The concept of critical stenosis is the degree of vessel occlusion beyond which there are abrupt changes in the flow properties. The secondary objective is to solve the problem with multiple constrictions in a tube by concentrating on a module at a sufficient distance downstream from the inlet where the flow is fully developed as the flow field becomes periodic and to find the relationship between the pressure drop across the module and the Reynolds number.

PROBLEM FORMULATION

The equations governing the flow in cylindrical co-ordinates are presented in the primitive variable form. Constant fluid properties are assumed and the flow is considered axisymmetric and laminar. The problems formulated are classified into two cases. The first case deals with tubes with up to four constrictions located equidistant from each other. Case 2 deals with the situation where there are a number of constrictions in the tube equidistant from each other and the problem is formulated for one module in the system. Primitive variable form of the governing equation is selected because it will be easier to extend the models to three dimensions and to turbulence.

Case 1. (Tube with multiple constrictions)

In this case there are one, two, three and four constrictions in the tube. The geometry of the model with four constrictions is shown in Figure 1. The pertinent geometrical characteristics of the models tested are summarized in Table I. The geometry of models M1, M2 and M3 are essentially the same as shown in Figure 1 except that model M1 has only the first constriction, model M2 has the first and second constrictions and model M3 has the first three constrictions. The equation used to generate the geometry of the model is of the following form

$$R = R_0 + \sum_{i=1}^{n} A \exp\left(-\frac{1}{2(0{\cdot}25S)^2}(x - d_i)^2\right), \tag{1}$$

where R is the radius of the tube at any location, d_i is the distance to the centre of each of the constrictions from the inlet of the tube and n is the total number of constrictions. The constrictions are located sufficiently apart from each other such that the shape of one of the constrictions have practically no influence on shape of the other constrictions.

The flow field solutions were obtained for all the models. The non-dimensional variables are defined as

$$\begin{gathered} u = u^*/V, \quad v = v^*/V, \quad x = x^*/D_0, \quad r = r^*/D_0, \\ p = p^*/\rho V^2, \quad Re = \rho V D_0/\mu, \end{gathered} \tag{2}$$

where the average velocity is taken as the reference velocity, V.

The governing equations are the mass conservation and the u and v momentum equations which are given as

Mass conservation equation

$$\frac{\partial u}{\partial x} + \frac{1}{r}\frac{\partial (rv)}{\partial r} = 0. \tag{3}$$

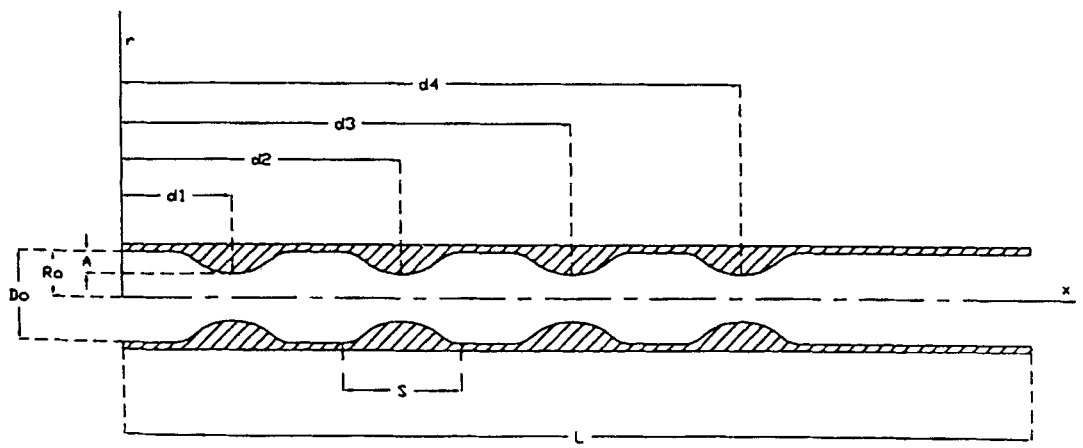

Figure 1. Geometry of the tube with constrictions (Case 1)

Table I. Geometries of the models

Model	Area reduction	No. of constrictions	*Re*	d1	*d*2	*d*3	*d*4
Case 1: M1	75%	1	50–250	3	—	—	—
M2	75%	2	50–250	3	9	—	—
M3	75%	3	50–250	3	9	15	—
M4	75%	4	50–250	3	9	15	21

Momentum conservation equations

$$\left[\frac{\partial(uu)}{\partial x}+\frac{1}{r}\frac{\partial(rvu)}{\partial r}\right]=\frac{1}{Re}\left[\frac{\partial^2 u}{\partial x^2}+\frac{1}{r}\frac{\partial}{\partial r}\left(r\frac{\partial u}{\partial r}\right)\right]-\frac{\partial p}{\partial x}, \tag{4}$$

$$\left[\frac{\partial(uv)}{\partial x}+\frac{1}{r}\frac{\partial(rvv)}{\partial r}\right]=\frac{1}{Re}\left[\frac{\partial^2 v}{\partial x^2}+\frac{1}{r}\frac{\partial}{\partial r}\left(r\frac{\partial v}{\partial r}\right)-\frac{v}{r^2}\right]-\frac{\partial p}{\partial r}. \tag{5}$$

The boundary conditions on the symmetry lines are

$$\frac{\partial u}{\partial r}=0, \qquad v=0. \tag{6}$$

On the solid bounding walls, the no slip boundary condition is used.

$$u=0, \qquad v=0 \quad \text{at} \quad r=R. \tag{7}$$

At the inlet the flow is assumed to be fully developed and laminar, therefore,

$$u=2(1-4r^2), \qquad v=0, \tag{8}$$

and at the exit, zero gradient boundary conditions are used.

$$\frac{\partial u}{\partial x}=0, \qquad \frac{\partial v}{\partial x}=0. \tag{9}$$

Case 2. Modular approach

The governing equations for the modular approach were formulated under the assumption that the fluid flow in a tube with a periodically varying cross section attains a fully developed regime, in the sense that the velocity field repeats itself at corresponding axial stations in successive cycles. Hence the governing equations for the fluid flow could be developed for a single isolated module without dealing with the entrance region problem. The geometry of such a module is shown in Figure 2. The periodic behaviour of velocity components is expressed as

$$u(x,r)=u(x+\lambda,r),\ v(x,r)=v(x+\lambda,r), \tag{10}$$

where x is any arbitrary location in the fully developed region and λ is length of the module (distance between the two constrictions). The cross-sectional pressure distributions at x and $x+\lambda$ are identical in shape, but the pressure level is lower in the downstream station. It then follows that

$$p(x,r)-p(x+\lambda,r)=p(x+\lambda,r)-p(x+2\lambda,r)=\ldots. \tag{11}$$

Defining the pressure drop across a module of length λ as

$$\frac{p(x,r)-p(x+\lambda,r)}{\lambda}=K, \tag{12}$$

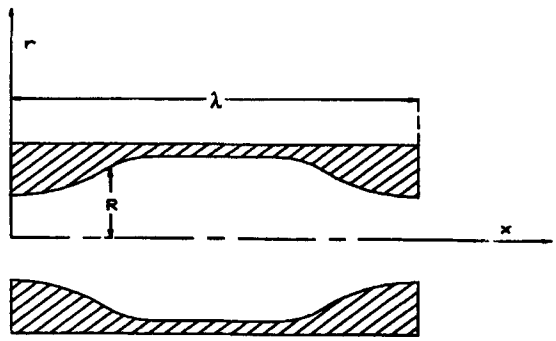

Figure 2. Geometry of the module

where K is a constant. This pressure field at any location (x, r) could be subdivided into two components

$$p(x, r) = -Kx + \bar{p}(x, r), \tag{13}$$

where $\bar{p}(x, r)$ is the periodic component the value of which is repetitive over successive modules and K is an assignable parameter, which is related to the average flow rate and Reynold's number. The periodic condition is expressed as

$$\bar{p}(x, r) = \bar{p}(x + \lambda, r). \tag{14}$$

The governing equations retain the same form as in Case 1, however, with the following modifications. The reference velocity, $V = \mu/(\rho D_0)$, is used and the pressure gradient terms that appear in the momentum equations are modified using equations (13) and (14). The boundary conditions at the wall and symmetry planes are the same as Case 1. At the inlet and exit, the periodicity conditions (Equations (10) and (14)) are used and the value for K is assigned

$$-\frac{\partial p}{\partial x} = K - \frac{\partial \bar{p}}{\partial x}, \qquad \frac{\partial p}{\partial r} = \frac{\partial \bar{p}}{\partial r}. \tag{15}$$

Transformation of basic equations

The tube, with constrictions, is mapped into a rectangular domain. The new co-ordinate system is defined as $\xi = \xi(x, r)$ and $\eta = \eta(x, r)$. The transformed computational domain is shown in Figure 3. The partial derivatives of any function f can be transformed as

$$f_x = \frac{(r_\eta f_\xi - r_\xi f_\eta)}{J}, \qquad f_r = \frac{(-x_\eta f_\xi + x_\xi f_\eta)}{J}, \tag{16}$$

where J is the Jacobian of the transformation:

$$J = x_\xi r_\eta - x_\eta r_\xi = \frac{1}{\xi_x \eta_r - \eta_x \xi_r}. \tag{17}$$

The governing equations, (3), (4) and (5), can be expressed as

$$\left[\frac{\partial(u\phi)}{\partial x} + \frac{1}{r}\frac{\partial(rv\phi)}{\partial r}\right] = \frac{1}{Re}\left[\frac{\partial^2 \phi}{\partial x^2} + \frac{1}{r}\frac{\partial}{\partial r}\left(r\frac{\partial \phi}{\partial r}\right)\right] + S^\phi, \tag{18}$$

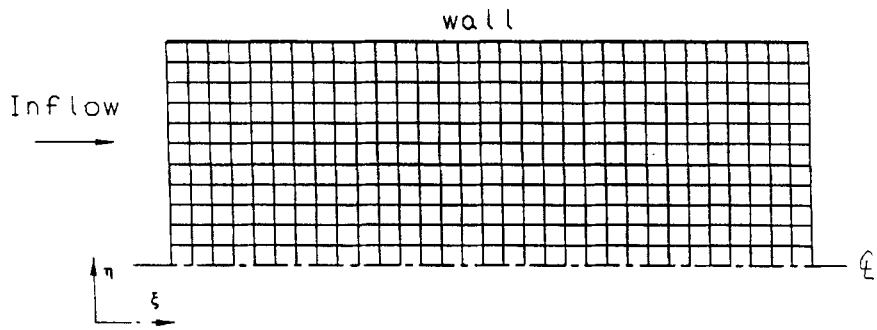

Figure 3. Computational domain

where $\phi = 1$, u or v for the mass conservation and x-component and r-component of momentum equations respectively. S^{ϕ} is the source term which is zero for the mass conservation equation. Employing the procedure of transformation as given by equation (16) on equation (18), the governing equations are transformed into the (ξ, η) co-ordinate system. The governing equation in the transformed coordinate system takes the following form

$$\frac{1}{J}\left(\frac{\partial}{\partial\xi}(ur_\eta\phi) - \frac{1}{r}\frac{\partial}{\partial\xi}(rvx_\eta\phi) + \frac{1}{r}\frac{\partial}{\partial\eta}(rvx_\xi\phi) - \frac{\partial}{\partial\eta}(ur_\xi\phi)\right)$$
$$= \frac{1}{ReJ}\left(\frac{\partial}{\partial\xi}\frac{1}{J}(r_\eta r_\eta)\phi_\xi + \frac{1}{r}\frac{\partial}{\partial\xi}\frac{1}{J}(rx_\eta x_\eta)\phi_\xi - \frac{\partial}{\partial\xi}\frac{1}{J}(r_\eta r_\xi)\phi_\eta - \frac{1}{r}\frac{\partial}{\partial\xi}\frac{1}{J}(rx_\eta x_\xi)\phi_\eta + \frac{\partial}{\partial\eta}\frac{1}{J}(r_\xi r_\xi)\phi_\eta\right.$$
$$\left. + \frac{1}{r}\frac{\partial}{\partial\eta}\frac{1}{J}(rx_\xi x_\xi)\phi_\eta - \frac{\partial}{\partial\eta}\frac{1}{J}(r_\xi r_\eta)\phi_\xi - \frac{1}{r}\frac{\partial}{\partial\eta}\frac{1}{J}(rx_\xi x_\eta)\phi_\xi\right) + S^{\phi}. \tag{19}$$

The terms containing derivatives with respect to the original independent variables in S^{ϕ} should also be transformed in terms of new independent variables. Hence for the x and r momentum conservation equations

$$S_v = -\frac{v}{Re\, r^2} + \frac{1}{J}(x_\eta p_\xi - x_\xi p_\eta),$$
$$S_u = \frac{1}{J}(-r_\eta p_\xi + r_\xi p_\eta). \tag{20}$$

For Case 2, S_u will have an additional term K and p is replaced with $\bar{p}$.

NUMERICAL METHOD OF SOLUTION

The present numerical scheme is similar to the SIMPLE method developed by Patankar and Spalding.[11] Rhie and Chow[12] used a curvilinear co-ordinate system which removed the geometric limitations of the SIMPLE method. The present method is a modified version of this as it involves transforming the governing equations from polar co-ordinates to curvilinear co-ordinates and adapts

the numerical scheme for this problem. A staggered grid arrangement is used for the solution and is shown in Figure 4. Integrating equation (19) over the control volume, the approximation of the integral conservation equation is written as

$$(G_1\phi\Delta\eta)_w^\theta + (G_2\phi\Delta\xi)_s^n = \left\{\frac{1}{J\,Re}(\alpha\phi_\xi - \beta_1\phi_\eta)\Delta\eta\right\}_w^\theta + \left\{\frac{1}{J\,Re}(\gamma\phi_\eta - \beta_2\phi_\xi)\Delta\xi\right\}_s^n + \frac{S^\phi}{\rho}J\Delta\xi\Delta\eta, \tag{21}$$

where G_1 and G_2 are directly related to the contravariant velocity components and

$$G_1 = ur_{\eta_p} - \frac{r}{r_p}vx_{\eta_p}, \qquad G_2 = \frac{r}{r_p}vx_{\xi_p} - ur_{\xi_p}, \tag{22}$$

$$\alpha = r_{\eta_p}r_\eta + \frac{r}{r_p}x_{\eta_p}x_\eta, \qquad \beta_1 = r_{\eta_p}r_\xi + \frac{r}{r_p}x_{\eta_p}x_\xi,$$
$$\beta_2 = r_{\xi_p}r_\eta + \frac{r}{r_p}x_{\xi_p}x_\eta, \qquad \gamma = r_{\xi_p}r_\xi + \frac{r}{r_p}x_{\xi_p}x_\xi. \tag{23}$$

A relation between the dependent variable 'ϕ' at point 'P' and its neighbouring points, E, W, N, S can then be obtained, i.e.

$$A_P\phi_p = A_E\phi_E + A_W\phi_W + A_N\phi_N + A_S\phi_S + S^\phi J\Delta\xi\Delta\eta - \left[\left(\frac{1}{Re\,J}\beta_1\phi_\eta\Delta\eta\right)_w^\theta + \left(\frac{1}{Re\,J}\beta_2\phi_\xi\Delta\xi\right)_s^n\right], \tag{24}$$

where the coefficients such as A_E involves convection and diffusion. The last two terms in the equation originated from the cross products of the diffusion terms and can be included in the source terms for numerical computation. Representing the source term as S it can be linearized as $S = S_c - S_p\phi_p$. The terms corresponding to S_p are combined with A_p while performing the calculations.

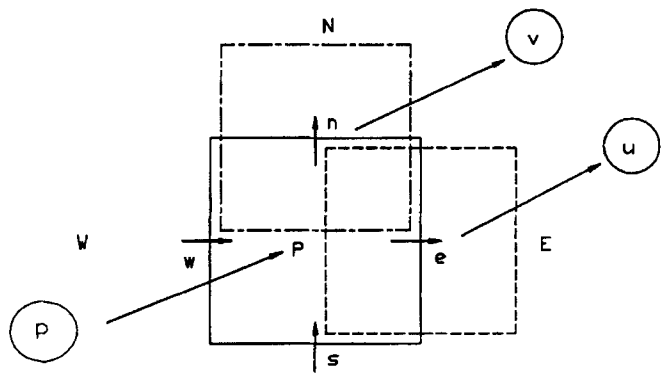

Figure 4. Staggered grid arrangement

The coefficients are calculated according to the 'power law scheme' which provides an accurate representation of the exact solution when applied to a one-dimensional problem and performs reasonably well in problems of higher dimensions. The power law scheme was found to be very robust and did not pose difficulties during convergence of the code. The scheme was also thoroughly checked in the model validation process to ensure that the results were reasonable and accurate. The reason why the power law scheme was selected although higher-order schemes like QUICK are more accurate is that they are prone to numerical instabilities and code convergence especially in problems with complicated domains such as the one studied and they are known to produce undershoots and overshoots.

The coefficients are expressed as

$$\begin{aligned} A_{\mathrm{E}} &= D_e \max(0, 1 - 0{\cdot}1|P_e|^5) + \max(-F_e, 0), \\ A_{\mathrm{W}} &= D_w \max(0, 1 - 0{\cdot}1|P_w|^5) + \max(F_w, 0), \\ A_{\mathrm{N}} &= D_n \max(0, 1 - 0{\cdot}1|P_n|^5) + \max(-F_n, 0), \\ A_{\mathrm{S}} &= D_s \max(0, 1 - 0{\cdot}1|P_s|^5) + \max(F_s, 0), \\ A_P &= A_{\mathrm{E}} + A_{\mathrm{W}} + A_{\mathrm{N}} + A_{\mathrm{S}} + S_p J \Delta\xi \Delta\eta, \qquad P = \frac{F}{D}, \end{aligned} \tag{25}$$

where

$$\begin{aligned} D_n &= \frac{1}{Re\, J} \gamma_\eta \frac{\Delta\xi}{\Delta\eta_n}, & F_n &= (G_2)_n \Delta\xi, \\ D_s &= \frac{1}{Re\, J} \gamma_s \frac{\Delta\xi}{\Delta\eta_s}, & F_s &= (G_2)_s \Delta\xi, \\ D_e &= \frac{1}{Re\, J} \alpha_e \frac{\Delta\eta}{\Delta\xi_e}, & F_e &= (G_1)_e \Delta\eta, \\ D_w &= \frac{1}{Re\, J} \alpha_w \frac{\Delta\eta}{\Delta\xi_w}, & F_w &= (G_2)_w \Delta\eta. \end{aligned} \tag{26}$$

The quantities such as G_{1e} and D_e are obtained by linear interpolation on the physical plane and the pressure correction terms are derived in a manner similar to the SIMPLE method.

The pressure correction equation is derived in a manner similar to the SIMPLE method. The correction equations for G_1 and G_2 are obtained by using the velocity and pressure corrections and equation (22) and neglecting the terms corresponding to p'_η in the equation for G_1 and those corresponding to p'_ξ in the equation for G_2. They are

$$G_1 = G_1^* + \bar{B} p'_\xi, \qquad G_2 = G_2^* + \bar{C} p'_\eta, \tag{27}$$

where $\bar{B} = B^u r_{\eta p} - (r/r_p) B^v x_{\eta p}$ and $\bar{C} = (r/r_p) C^v X_{\xi p} - C^u r_{\xi p}$. The pressure correction equation can be obtained by substituting equation (27) into the mass conservation equation (3).

The pressure correction equation takes the form

$$\begin{aligned} &(G_1^* \Delta\eta)_\theta - (G_1^* \Delta\eta)_w + (G_2^* \Delta\xi)_\eta - (G_2^* \Delta\xi)_w + \\ &(\bar{B} p'_\xi \Delta\eta)_\theta - (\bar{B} p'_\xi \Delta\eta)_w + (\bar{C} p'_\eta \Delta\xi)_n - (\bar{C} p'_\eta \Delta\xi)_s = 0 \end{aligned} \tag{28}$$

A relationship for the variable p' at point P and its neighbouring points, E, W, N, S can be obtained and given as

$$A_P^p p'_p = A_{\mathrm{E}}^p p'_{\mathrm{E}} + A_{\mathrm{W}}^p p'_{\mathrm{W}} + A_{\mathrm{N}}^p p'_{\mathrm{N}} + A_{\mathrm{S}}^p p'_{\mathrm{S}} + m_p, \tag{29}$$

where

$$
\begin{aligned}
A_{\mathrm{N}}^{p} &= \bar{C}\frac{\Delta\xi}{\Delta\eta}\bigg|_{n}, \qquad A_{\mathrm{S}}^{p} = \bar{C}\frac{\Delta\xi}{\Delta\eta}\bigg|_{s}, \\
A_{\mathrm{E}}^{p} &= \bar{B}\frac{\Delta\eta}{\Delta\xi}\bigg|_{e}, \qquad A_{\mathrm{W}}^{p} = \bar{B}\frac{\Delta\eta}{\Delta\xi}\bigg|_{w}, \\
A_{P}^{p} &= A_{\mathrm{E}}^{p} + A_{\mathrm{W}}^{p} + A_{\mathrm{N}}^{p} + A_{\mathrm{S}}^{p}, \\
m_{p} &= (G_{1}^{*}\Delta\eta)_{e} - (G_{1}^{*}\Delta\eta)_{w} + (G_{2}^{*}\Delta\xi)_{\eta} - (G_{2}^{*}\Delta\xi)_{s}.
\end{aligned}
\tag{30}
$$

The solution procedure is the same as the SIMPLE method. For Case 2 a periodic tridiagonal solver was used due to the periodicity boundary conditions.

Grid dependency tests were carried out using grid sizes of 150 × 15, 200 × 20, 250 × 25 and 300 × 30 for Case 1. Grid sizes of 250 × 25 and 300 × 30 yielded similar results indicating that the solution has become grid independent and a grid size of 300 × 30 was selected for the study. Similarly for Case 2, grid dependency tests were carried out using grid sizes of 20 × 15, 30 × 20, 35 × 25 and 40 × 30. A grid size of 40 × 30 was selected as the results had become grid independent for this size.

Modelling the problem in curvilinear co-ordinates enables a wide variety of parameters to be varied. For this study, the fluid selected was water. For Case 2 the length of the module was taken to be a non-dimensional value of 6 corresponding to the distance between the constrictions in Case 1, while all the other parameters remained the same as in Case 1.

MODEL VALIDATION

The model was compared with several known experimental results before applying it to the problem of interest. The amplitude of the constrictions in the numerical model was made negligible and the friction factors were compared with pipe flow results. This comparison is shown in Figure 5. Young and Tsai[1] conducted steady flow experiments and computed pressure drop measurements across single constriction for various models of stenosis. The fluid used was water. The unconstricted diameter of the tube was 0·744 inches. Two test cases were selected for comparison. One had an 89 per cent constriction and a spread of the constriction, S, four times the tube diameter and the other with 89 per cent constriction and the spread of the constriction was twice the tube diameter. The spread of the constriction is shown in Figure 1. The pressure taps were located 6 in either side of the constriction. The results of these comparisons with the present model are shown in Figure 6.

Velocity measurements in a tube with a single constriction were performed by Ahmed and Giddens[3] using a Laser Doppler Anemometer. The tube internal diameter was 2 in and the spread of the constriction was twice the tubes internal diameter. The fluid used had a kinematic viscosity of 0·12 stokes. The measurements were taken in tubes with 25 per cent and 75 per cent area reduction. A comparison is made with the present results for a Reynolds number of 500 at the distances of z equalling 0 and 2·5, where z is the distance from the centre of the constriction in Figure 7. For the 75 per cent constriction, the experiments indicated that the flow field showed an oscillation in the shear layer and was beginning to become turbulent which may be the cause of discrepancy in the results.

The agreement between the current numerical method and the experiments serves to validate the method. The next section includes a comparison of the flow solution in a tube having multiple constrictions with the solution obtained by assuming periodicity conditions in a module (Case 2).

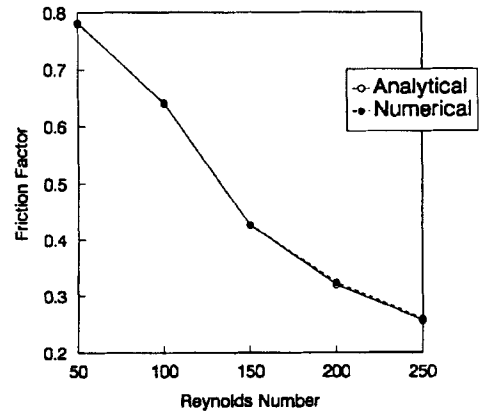

Figure 5. Comparison of numerical and analytical results for pipe flow

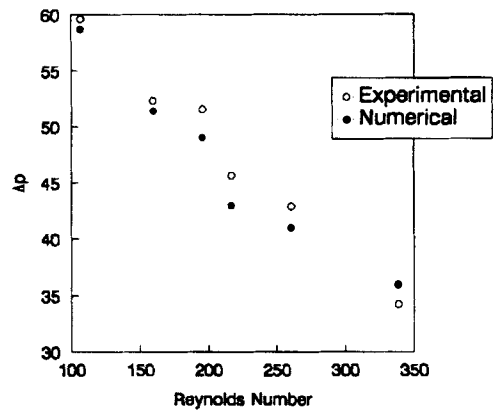

(a) $S_c = 4D_o$

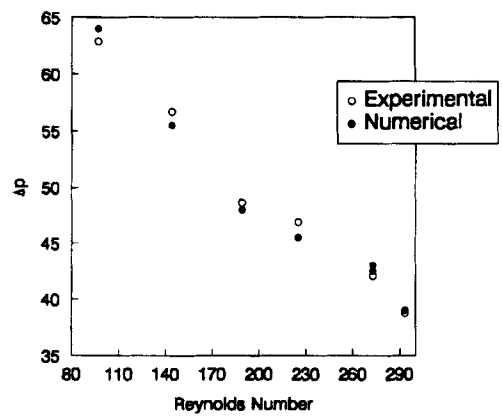

(b) $S_c = 2D_o$

Figure 6. Comparison of non-dimensional pressure drop across stenosis

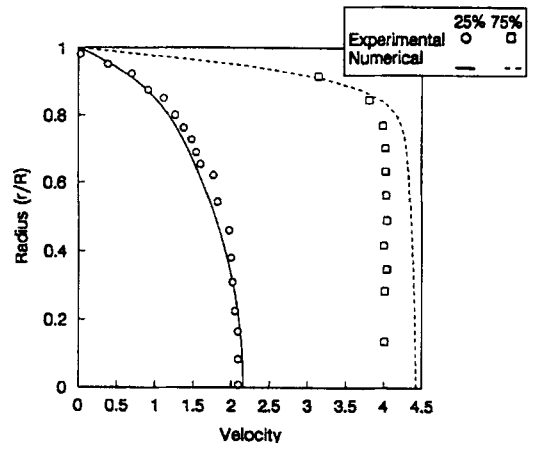

Figure 7. Comparison of non-dimensional velocity

RESULTS AND DISCUSSION

The characteristics of the flow were investigated for Reynolds numbers of 50–250 for models having one, two, three and four constrictions in the tube (models M1, M2, M3 and M4 in Case 1). The spread of the constriction (S) was taken to be twice the tube diameter. Other pertinent geometric characteristics of the models studied are shown in Table I. The maximum value of 250 was selected for the Reynolds number to ensure that the flow remains laminar. For the modular approach (Case 2) a sample model is solved corresponding to a Reynolds number of 200.

Case 1

Pressure. The pressure flow relationship is one means of obtaining information about the severity of a coronary stenosis. For a given Reynolds number the presence of a constriction increases the resistance that the flow experiences. The pressure drop across the constrictions for the various models

are shown in Figure 8. It can be seen that the pressure drop increases as the number of constrictions increases. The non-dimensional pressure drop for each of the models, in a manner similar to Poiseuille flow, decreases as the Reynolds number increases.

The non-dimensional pressure distribution along the tube wall in the axial direction, is also of interest. A sample plot is shown in Figure 9 for a tube with four constrictions and for a range of Reynolds numbers. There is a rapid fall in the pressure as the occlusion is approached, with pressure recovery taking place over a greater length. As the number of constrictions is increased, the development of the periodic nature of the flow can be seen. The curves show a similar pressure drop and recovery across every constriction even as they are shifted correspondingly downwards. This shift is due to the mass flow in the positive x direction.

Velocity. A sample plot of the variation of centreline velocity, in the axial direction for the range of Reynolds numbers is shown in Figure 10 for a tube with four constrictions. It could be seen that the maximum centreline velocity occurs slightly downstream of the constriction due the formation of a recirculation zone near the wall as a result of flow separation. This effectively reduces the cross-sectional area of the flow. The centreline velocity is seen to take a larger distance to recover its initial value as the Reynolds number increases. As the number of constrictions increases, the fluid does not have an opportunity to recover to its initial value of the velocity before it encounters another constriction. Only for low Reynolds numbers does the fluid have time to recover. For lower Reynolds number, the velocity field is such that it is independent of the other constrictions.

Wall shear stress, vorticity and streamlines. The wall shear stress, τ_w, is an important parameter in atherosclerosis. Figure 11 shows the nature of the wall shear stress variation in the axial direction for the case of a tube with four constrictions. The peak value of τ_w increases with an increase in Reynolds number. The wall shear stress value increases rapidly as the flow approaches the constriction and reaches a peak value near the maximum constricted area. Downstream of the constriction τ_w decreases rapidly and reverses sign which indicates a separation in the flow near the wall of the tube. An increase in Reynolds number causes the magnitude of the negative τ_w value to increase downstream of the constriction. This is due to an increase in the size of the recirculation region. The wall vorticity is very similar to τ_w as they are directly related in Newtonian flows. The maximum value of wall shear generated by the first constriction is always greater than the maximum value of

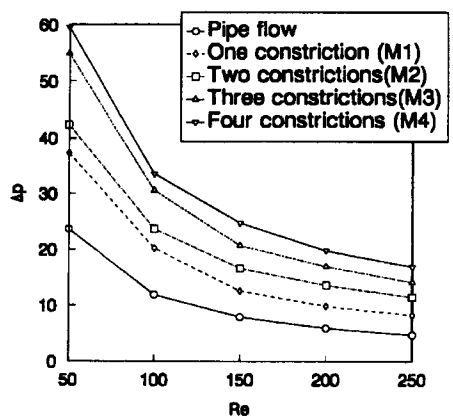

Figure 8. Non-dimensional pressure drop across the constrictions

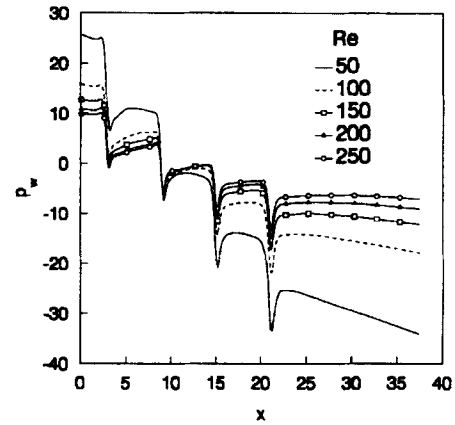

Figure 9. Non-dimensional pressure distribution along the wall

wall shear generated by the second constriction. This is because the recirculation eddy formed downstream of the first constriction has a diminishing effect on the vortices generated by the main stream near the second constriction area. However, an increase in the number of constrictions causes a tendency for the periodic nature of the flow to develop and hence the wall shear stress to behave similarly for the other constrictions. The peak value of wall shear stress which is slightly higher in the vicinity of the last constriction may be attributed to the presence of no other constrictions downstream.

The contours of vorticity and streamlines are shown for a Reynolds number of 200 for all the models in Figures 12 and 13. There is a recirculation eddy downstream of each constriction. The recirculating eddies divide the flow into two regimes one of which is the recirculating region, and the other is the main flow field carrying the bulk of the flow near the centre of the tube.

Periodic nature of the flow. The development of the periodic nature of the flow were studied by simulating the flow passing through a tube with seven constrictions. The results were compared for a

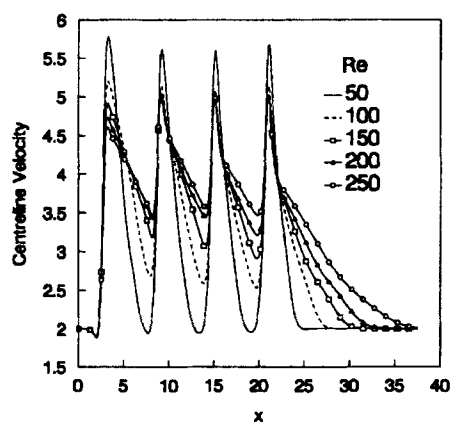

Figure 10. Non-dimensional centreline velocity distribution

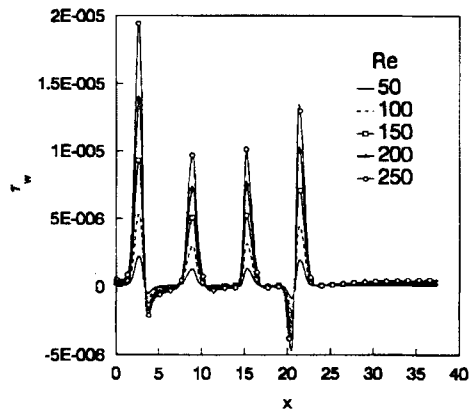

Figure 11. Non-dimensional wall shear stress distribution

range of Reynolds numbers between 50 to 250. As the Reynolds number is increased the flow is expected to reach its fully developed state after a larger number of constrictions.

The results were shown by comparing the wall shear stress profiles between the constrictions by plotting them on top of one another. The space between the constriction is referred to as a module. For example 'module 1' is between constriction 1 and 2. The profiles are shown in Figure 14. The development of the periodic nature of the flow could be clearly seen from the results. The flow pattern repeats itself after the second module for lower Reynolds numbers and after the third module for higher Reynolds numbers. An approximate expression for the periodic development length for a laminar flow could be obtained for a problem having a similar geometry and inlet conditions as studied in this work, i.e.

$$n_m = \frac{l_e}{D_0} \geq 1 + \left[\!\left[\frac{Re}{100} + 1\right]\!\right], \tag{31}$$

where the function $[\![\ ]\!]$ is the greatest integer function and n_m refers to the number of modules and l_e is the entrance length.

Case 2

The previous results indicate the development of periodic characteristics of the flow as the number of similar constrictions increases in the streamwise direction. The flow field under such conditions can be solved by isolating the problem in a single module corresponding to the fully developed region in the duct. For this problem periodic boundary conditions must be applied at the inlet and outlet of the module. The pressure drop across the module, K, is an assignable parameter which corresponds to a particular value of the Reynolds number. The value of the Reynolds number corresponding to the unconstricted tube diameter could only be found only after the model is solved by performing a numerical integration of the following form at any axial location in the module where the diameter is D_0 (unconstricted tube diameter).

$$Re_m = \frac{4}{v\pi D_0} \int_0^{0.5D_0} u(r) 2\pi r \mathrm{d}r, \tag{32}$$

(a) one constriction

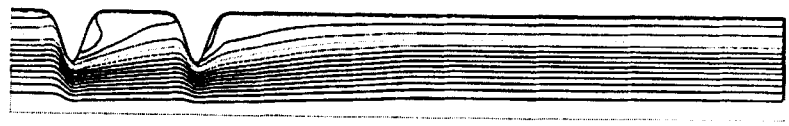

(b) two constrictions

(c) three constrictions

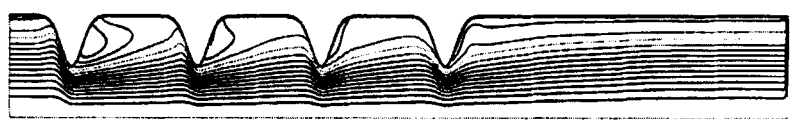

(d) four constrictions

Figure 12. Streamline profiles

where $u(r)$ is the velocity at r, for this particular axial location. The model was solved for various values of K and the corresponding Reynolds numbers were obtained using equation (32). These results are shown in Figure 15. The model validated by comparing the results of the centreline velocity profile and wall shear stress with module 4 (between third and fourth constriction) in the tube having seven constrictions for a Reynolds number of 200. The results of the comparison are shown in Figures 16 and 17 which indicates the model performs reasonably well. Sample plots of streamfunction and vorticity are also shown for a Reynolds number of 200 in Figures 18 and 19. The results are similar to those discussed in Case 1.

(a) one constriction

(b) two constrictions

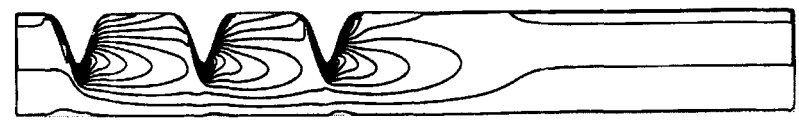

(c) three constrictions

(d) four constrictions

Figure 13. Vorticity contours

CONCLUSIONS

The flow field in the neighbourhood of multiple axisymmetric constrictions were investigated for a range of Reynolds numbers between 50 to 250. Constrictions with 75 per cent reduction in the flow area were used for the present study. The problem was formulated in curvilinear co-ordinates due to the flexibility that the approach provides regarding the shape and the number of constrictions in the pipe. A detailed description of the conversion of governing equation from cylindrical co-ordinates to curvilinear co-ordinates was provided along with the numerical scheme. The effect that number of constrictions had on the flow characteristics such as pressure drop and wall shear stress were studied in detail. The development of the periodicity characteristics of the flow were observed and an approximate expression for the development region required to achieve the periodically fully developed state was shown. This expression is valid only for problems of similar geometry and for Reynolds number below 250 as the flow remains laminar in this regime. The presence of the periodic

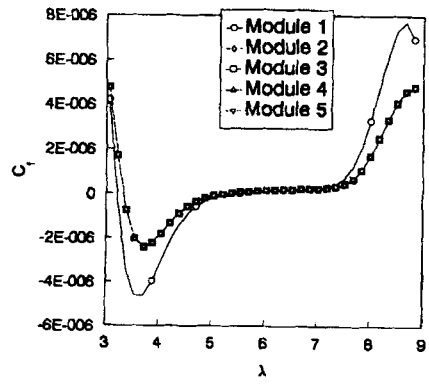

(a) Re = 50

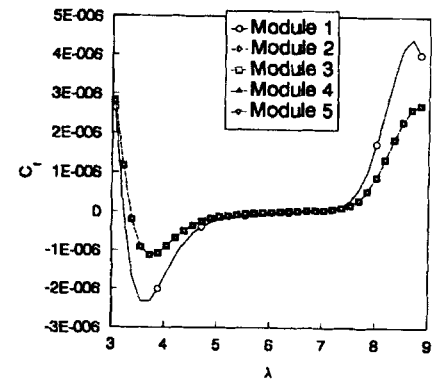

(b) Re = 100

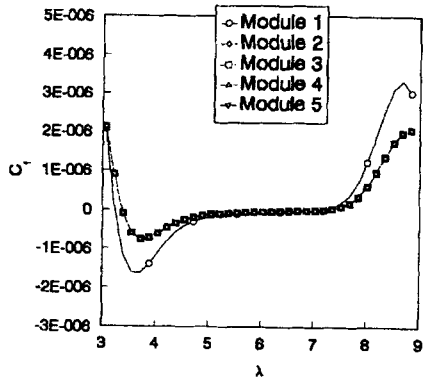

(c) Re = 150

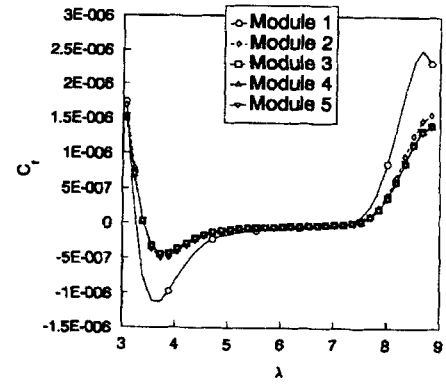

(d) Re = 200

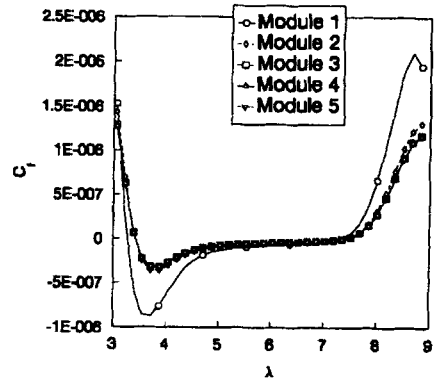

(e) Re = 250

Figure 14. Comparison of skin friction coefficient across the modules

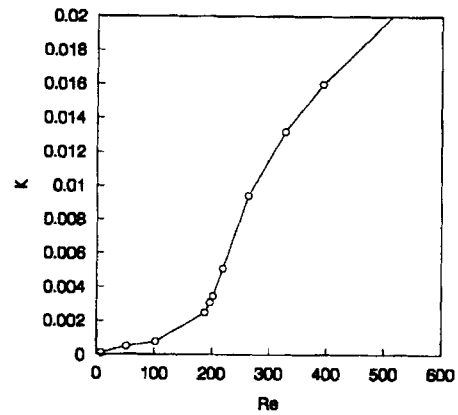

Figure 15. Non-dimensional pressure drop across the module versus Reynolds number

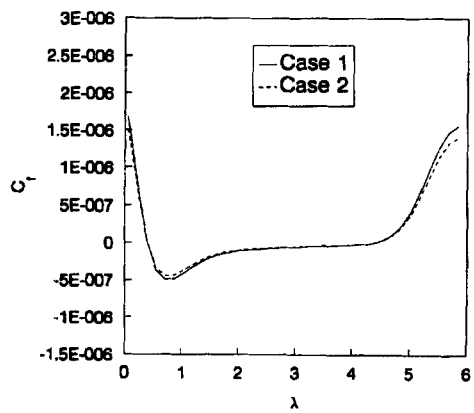

Figure 16. Comparison of skin friction coefficients (Case 1 versus Case 2)

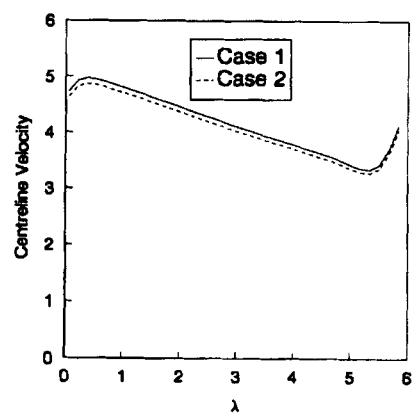

Figure 17. Comparison of non-dimensional centreline velocity (Case 1 versus Case 2)

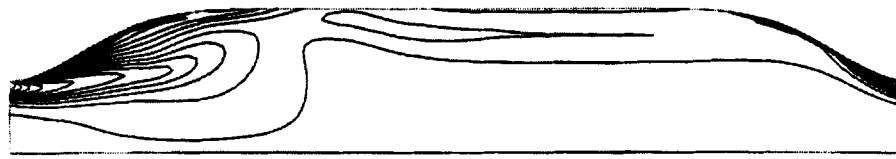

(b) Case 2

Figure 18. Vorticity contours (Case 2)

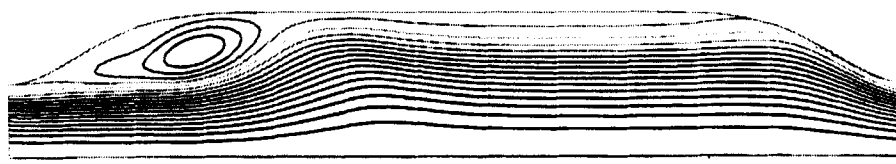

(b) Case 2

Figure 19. Streamline profiles (Case 2)

nature of the flow indicated that the flow characteristics could be provided in the periodically fully developed region by solving the problem for one isolated module in that regime. The governing equation in curvilinear co-ordinates and the numerical scheme were developed for the modular approach using periodicity boundary conditions and the pressure drop across the module, K, as an assignable parameter. The Reynolds number for the flow corresponding to the unconstricted tube diameter was found for various values of K. A similar approach could be used in providing flow field solutions in some heat transfer systems such as a reflux condenser which has a geometry similar to the problem solved. The computational results can be an essential first step in studying blood flow in the presence of stenosis where the pressure drop across the stenosis and the wall shear stresses are of considerable importance. However, the present approach should be extended to include unsteady terms and wall motions. This would provide a significant improvement over the present model as the pulsatile nature of the flow and the instabilities caused by it could be investigated.

ACKNOWLEDGEMENT

This research work was financially supported through a University of Windsor Postgraduate Scholarship and grants from the Natural Sciences and Engineering Research Council of Canada (Grant Numbers: OGP0001403 and OGP0105727).

APPENDIX: NOMENCLATURE

A	height of the constriction
A_E, A_W, A_N, A_S, A_P	coefficients in the general finite volume equations
D	diffusion conductance
D_0	unconstricted diameter of the tube
$d1$, $d2$, $d3$, $d4$	distances of the first, second, third and fourth constrictions from the inlet plane
F	flow rate through a control volume face
G_1, G_2	convective terms normal to grid cell boundaries

L	length of the tube
l_e	entrance length for a periodic fully developed flow
n_m	number of modules
P	Peclet number
p	non-dimensionalized pressure
p^*	pressure
r^*, x^*	radial and axial co-ordinates
r, x	non-dimensional radial and axial co-ordinates
R	radius of the tube
R_0	unconstricted radius of the tube
Re	Reynold's number ($=\rho V D_0/\mu$)
S	spread of the constriction
S^ϕ	average value of the of the source term over the control volume
V	reference velocity
u^*, v^*	x and r components of velocities
u, v	x and r components of non-dimensional velocities
z	non-dimensional distance from the centre of the constriction
α, β_1, β_2, γ	co-ordinate transformation parameters
K	pressure drop across a module
λ	length of the module
$\Delta\xi,\xi\eta$	cell boundary sizes in ξ and η directions in the transformed plane
μ	laminar viscosity
ν	kinematic viscosity
ξ, η	non-dimensional curvilinear co-ordinates
ρ	density
τ	shear stress
τ_w	wall shear stress
ϕ	general dependent variable

Subscripts

E, W, N, S	grid points (east, west, north, south)
e, w, n, s	control volume faces (east, west, north, south)
P	central grid point under consideration

REFERENCES

1. D. F. Young and F. Y. Tsai, 'Flow characteristics in models of arterial stenosis-I. Steady flow', *J. Biomech.*, **6**, 395–410 (1973).
2. N. Talukder, P. E. Karayannacos, R. M. Nerem and J. S. Vasco, 'An experimental study of fluid mechanics of arterial stenosis', *ASME J. Biomech. Engng*, **99**, 74–82 (1977).
3. S. A. Ahmed and D. P. Giddens, 'Velocity measurements in steady flow through axisymmetric stenosis at moderate Reynolds numbers', *J. Biomech.*, **16**, 505–516 (1983).
4. J. S. Lee and Y. C. Fung, 'Flow in locally constricted tubes at low Reynolds numbers', *ASME J. Appl. Mech.*, **37**, 9–16 (1970).
5. M. D. Deshpande, D. P. Giddens and R. F. Mabon, 'Steady laminar flow through modelled vascular stenosis', *J. Biomech.*, **9**, 165–174 (1976).
6. S. C. van Dreumel and G. D. C. Kuiken, 'Steady flow through a double converging–diverging tube model for mild coronary stenosis', *ASME J. Biomech. Engng*, **111**, 212–221 (1989).
7. T. S. Lee, 'Numerical studies of fluid flow through tubes with double constrictions', *Int. j. numer. meth. fluids*, **11**, 1113–1126 (1990).

8. E. M. Sparrow and A. T. Prata, 'Numerical solutions of laminar flow and heat transfer in a periodically converging–diverging tube', *Numer. Heat Transfer*, **6**, 441–461 (1983).
9. A. T. Prata and E. M. Sparrow, 'Heat transfer and fluid flow characteristics for an annulus of periodically varying cross-section', *Numer. Heat Transfer*, **7**, 285–304 (1984).
10. S. V. Patankar, C. H. Liu and E. M. Sparrow, 'Fully developed flow and heat transfer in ducts having streamwise-periodic variations of cross-sectional area', *ASME J. Heat Transfer*, **99**, 180–186 (1977).
11. S. V. Patankar and D. B. Spalding, 'A calculation procedure for heat, mass and momentum transfer in three-dimensional parabolic flow', *Int. J. Heat Mass Transfer*, **15**, 1787 (1972).
12. C. M. Rhie and W. L. Chow, 'Numerical study of turbulent flow past an airfoil with trailing edge separation', *AIAA J.*, **21**, 1525–1532 (1983).